

M. R. J. Palosaari¹, K. M. Kinnunen¹, M. L. Ridder², J. van der Kuur², H. F. C. Hoevers² and I. J. Maasilta¹

Analysis of impedance and noise data of an X-ray transition-edge sensor using complex thermal models

21.11.2011

Keywords TES, thermal model, impedance, noise

Abstract The so-called excess noise limits the energy resolution of transition-edge sensor (TES) detectors, and its physical origin has been unclear, with many competing models proposed. Here we present the noise and impedance data analysis of a rectangular X-ray Ti/Au TES fabricated at SRON. To account for all the major features in the impedance and noise data simultaneously, we have used a thermal model consisting of three blocks of heat capacities, whereas a two-block model is clearly insufficient. The implication is that, for these detectors, the excess noise is simply thermal fluctuation noise of the internal parts of the device. Equations for the impedance and noise for a three-block model are also given.

PACS numbers: 85.25.Oj, 85.25.Am, 74.25.fc, 74.40.Gh

1 Introduction

Calorimeters and bolometers based on superconducting transition-edge sensors (TES) have proven to be valuable tools in a number of applications in a broad energy range¹. The number of pixels in TES detector arrays are constantly increasing and the limits of single pixel performance are being pushed closer to the theoretical limits. However, the lack of understanding of some of the noise components ("excess noise") has plagued the field in recent years^{2,3}. One source for the excess noise, in addition to the recently introduced non-equilibrium Johnson noise⁴, could be a complex thermal circuit of the device: if the device consists of several blocks of heat capacity, more thermal fluctuation noise will exist^{5,6}. To

1: Nanoscience Center, Department of Physics, P. O. Box 35, FI-40014 University of Jyväskylä, Finland

E-mail: mikko.palosaari@jyu.fi

2: SRON Netherlands Institute for Space Research, Sorbonnelaan 2, 3584 CA Utrecht, the Netherlands

determine unambiguously the thermal noise components of the device, the thermal circuit should be determined independently. This can be done by measuring the complex impedance in addition to the noise⁷. For the device discussed here, the impedance data is fit well by a three-block thermal model, and the model simultaneously explains all the noise of the device. Thus, all noise sources are fully understood in the detector types presented here.

2 Theoretical models

To fully characterize the thermal and electrical properties of many TES devices, the conventional thermal model of one heat capacity connected to a heat bath is too simple. Even the model with one additional thermal block does not always fully fit the measured noise and impedance^{8,9}. Here we have used a system of three thermal blocks. We have analyzed the measured data with two different variations: one with both a hanging and an extra intermediate block between the TES and the heat bath, and another with two hanging thermal blocks (Fig. 1). The derivation

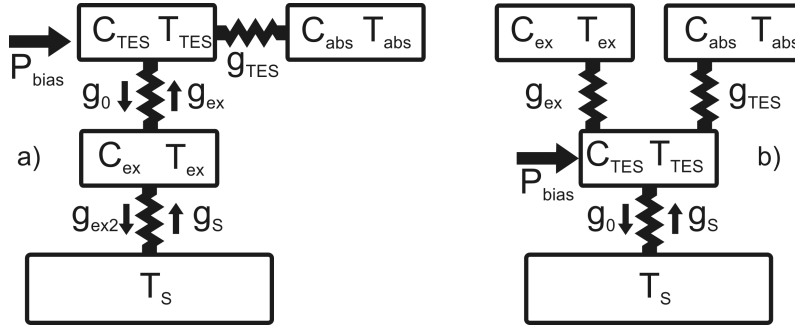


Fig. 1 a) A model with one hanging and an intermediate block between the TES and the bath (IH model). b) A model with two hanging thermal blocks (2H model).

and full theoretical discussion of the impedance and noise of the three-block models will be presented elsewhere¹⁰, here we only cite the results for the IH model (Fig. 1 a). Equations for 2H model (Fig. 1 b) are similar. The IH model assumes that heat flows first from the TES to the "intermediate" or excess heat capacity C_{ex} , and only then to the heat bath, therefore the steady state temperatures of the TES and the excess heat capacity are not equal. The hanging heat capacity C_{abs} could represent the absorber, but does not in general need to do so, and in steady state it has the same temperature as the TES. There are now five different dynamical thermal conductances that need to be defined, one between the TES and the "absorber", two between the TES and the excess heat capacity and two between the excess heat capacity and the bath: $g_{TES} = nAT_{TES}^{n-1}$, $g_0 = mBT_{TES}^{m-1}$, $g_{ex} = mBT_{ex}^{m-1}$, $g_{ex2} = pCT_{ex}^{p-1}$, $g_s = pCT_s^{p-1}$, where the power between the TES and the absorber, the TES and the excess heat capacity, and the excess heat capacity and the bath are given by $P = A(T_{TES}^n - T_{abs}^n)$, $P = B(T_{TES}^m - T_{ex}^m)$ and $P = C(T_{ex}^p - T_s^p)$, respectively (see Fig. 1).

2.1 Complex Impedance

The complex impedance of the model (Fig. 1 a) is

$$Z_{TES} = R_0(1 + \beta) + \frac{\mathcal{L}}{1 - \mathcal{L}} \frac{R_0(2 + \beta)}{1 + i\omega\tau_I - A(\omega) - B(\omega)}, \quad (1)$$

where $A(\omega) = \frac{1}{1 - \mathcal{L}} \frac{g_{tes}}{(g_{tes} + g_0)} \frac{1}{1 + i\omega\tau_{abs}}$, $B(\omega) = \frac{1}{1 - \mathcal{L}} \frac{g_0 g_{ex}}{(g_{tes} + g_0)(g_{ex} + g_{ex2})} \frac{1}{1 + i\omega\tau_{ex}}$, $\mathcal{L} = P_0\alpha / [(g_{tes} + g_0)T_0]$, $\tau_I = C_{tes} / [(g_{tes} + g_0)(1 - \mathcal{L})]$, $\tau_{abs} = C_{abs} / g_{tes}$ and $\tau_{ex} = C_{ex} / (g_{ex} + g_{ex2})$, and the transition steepness parameters are $\alpha = \partial \log(R) / \partial \log(T)$, $\beta = \partial \log(R) / \partial \log(I)$ at the bias point R_0 (with power P_0 and temperature T_0).

2.2 Noise

Three major classes of unavoidable noise sources are included: the power fluctuations in the thermal circuit, the electrical thermal noise of the detector (Johnson noise), and the Johnson noise of the shunt resistor. We disregard correlations between fluctuations in the thermal conductances.

The frequency dependent current responsivity, $s_I(\omega) = I_\omega / P_\omega$, for power input in the TES heat capacity C_{tes} can be written¹⁰ as

$$s_I(\omega) = -\frac{1}{Z_{circ}I_0} \frac{Z_{TES} - R_0(1 + \beta)}{R_0(2 + \beta)}, \quad (2)$$

where $Z_{circ} = Z_{TES} + R_L + i\omega L$, R_L is the Thevenin equivalent circuit resistance (shunt+parasitic) and L is the circuit inductance.

Now the thermal fluctuation current noise terms (one phonon noise term and two internal thermal fluctuation noise (ITFN) terms) are

$$|I|_{ph}^2 = P_{ph}^2 |s_I(\omega)|^2 \frac{g_{ex}^2}{(g_{ex} + g_{ex2})^2} \frac{1}{1 + \omega^2 \tau_{ex}^2}, \quad (3)$$

$$|I|_{ITFN,1}^2 = P_{tes}^2 |s_I(\omega)|^2 \frac{\omega^2 \tau_{abs}^2}{1 + \omega^2 \tau_{abs}^2}, \quad (4)$$

$$|I|_{ITFN,2}^2 = P_{ex}^2 |s_I(\omega)|^2 \frac{g_{ex2}^2 / (g_{ex2} + g_{ex})^2 + \omega^2 \tau_{ex}^2}{1 + \omega^2 \tau_{ex}^2}, \quad (5)$$

$$(6)$$

where $P_{ph}^2 = 2k_B(T_{ex}^2 g_{ex2} + T_s^2 g_s)$, $P_{tes}^2 = 4k_B T_0^2 g_{tes}$ and $P_{ex}^2 = 2k_B(T_0^2 g_0 + T_{ex}^2 g_{ex})$.

The non-equilibrium Johnson current noise in the TES film is given by

$$|I|_J^2 = \frac{V_\omega^2}{|Z_{circ,\infty} + \frac{\mathcal{L}(R_0 - R_L - i\omega L)}{1 + i\omega\tau_{tes} - (1 - \mathcal{L})(A(\omega) + B(\omega))}|^2}, \quad (7)$$

where⁴ $V_\omega^2 = 4k_B T_0 R_0(1 + 2\beta)$ and $Z_{circ,\infty} = R_0(1 + \beta) + R_L + i\omega L$. The Johnson noise due to the shunt and parasitic resistances is simply $|I|_{sh}^2 = V_{\omega,sh}^2 / |Z_{circ}|^2$, with $V_{\omega,sh}^2 = 4k_B T_{sh} R_L$ if both the parasitic resistance and the actual shunt are at temperature T_{sh} .

3 Experiments and Analysis

The measured TES was a pixel from an X-ray array fabricated at SRON (Fig. 2). It features a $206 \times 162 \times 1 \mu\text{m}^3$ Cu absorber on top of a SiOx insulator that is coupled to the TES through seven rectangular vias at the center of the TES. There are also 10×7 Cu dots of $10 \mu\text{m}$ diameter on top of the TES film (but not in contact with the absorber) to tune the transition properties. The critical temperature, T_C , is 125.5 mK and normal state resistance $R_N \sim 300 \text{ m}\Omega$. Measurements were performed in a compact plastic dilution refrigerator at Jyväskylä, with an old NIST SQUID readout¹¹ and a FLL electronics unit designed at SRON. The complex impedance was measured up to 100 kHz, taking into account of the transfer function of the readout circuit¹².



Fig. 2 (Color online) Left: Schematic cross-sectional view of the device. Orange: Cu absorber and dots, blue: SiOx insulator, gray: Ti layers, yellow: Au layer, black: Nb contacts. Right: Optical micrograph of the TES. The size of the Ti/Au TES is $186 \times 150 \mu\text{m}^2$ and it is on a $1 \mu\text{m}$ thick SiN membrane fabricated on Si (110) surface.

In the analysis, the measured complex impedance and noise were fitted simultaneously by eye with the equations described above, as high-dimensional non-linear least-squares fitting would be demanding to implement. The heat capacities, g_0 , g_{TES} and T_{ex} were free parameters. The other thermal conductances were calculated using the constraint that the total thermal conductance to the bath is fixed by the I-V data and that the links on both sides of the intermediate block have the same thermal exponent $p = m$. This is physically reasonable if all the conductances are dominated by the SiN membrane. During the fitting four curves were plotted on top of the experimental data: The noise as a function of frequency, the complex impedance and also the real and imaginary parts of the impedance as a function of frequency. White noise of $4 \text{ pA}/\sqrt{\text{Hz}}$ for the SQUID was included in the noise analysis.

4 Results and Discussion

One can fit all the major noise and impedance features with both three-block models (IH and 2H, Fig. 1), whereas a simpler two-block model (TES + hanging C) cannot produce an adequate fit, as can be seen in Fig. 3. In Fig. 4 the measured data and fitted theoretical curves for the IH model are presented. In the noise data, one can see that there is some deviation with the measured and the fitted data above 100 kHz. This is likely because the transfer function of the circuit was not corrected for in the noise data. We also analysed the measured data with the two

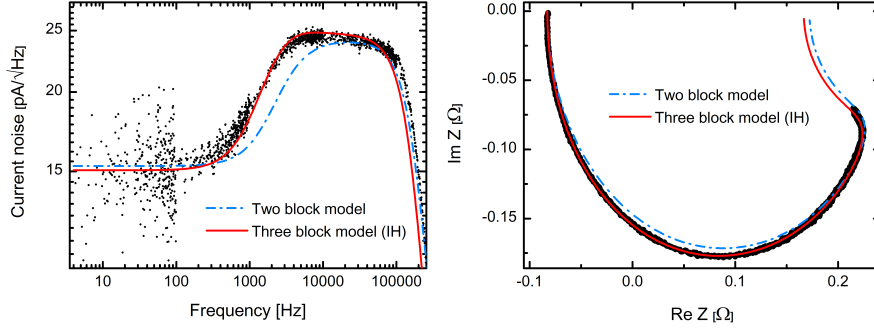


Fig. 3 (Color online) Comparison between a two-block model and the IH three-block model at 20% R/R_N .

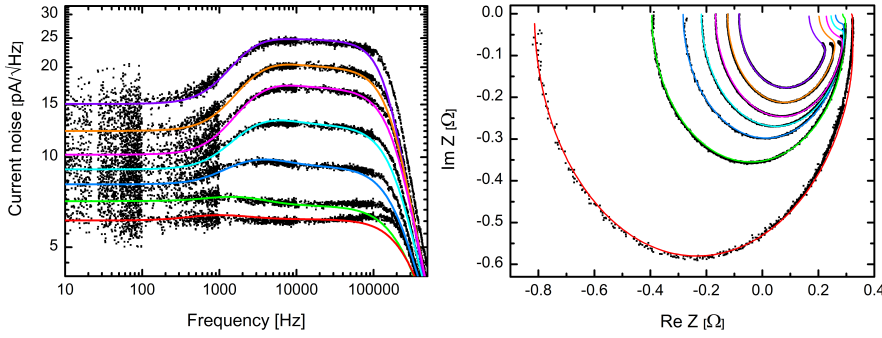


Fig. 4 (Color online) Left: the measured and fitted current noise of the device. Right: the measured and fitted complex impedance of the TES. Bias points between 20%-80% R_N in 10% intervals are presented. The higher bias points correspond to the lower noise levels and bigger semicircles. Only IH model fits are shown, 2H fits look identical.

hanging (2H) block model of Fig. 1 b) and obtained qualitatively identical goodness of fit results with the IH model. The fitted parameter values for both models are plotted in Fig. 5, except for C_{ex} in the 2H model which was approximately constant $C_{ex} \approx 0.08$ pJ/K. We also estimated the theoretical heat capacity of the Cu absorber, $C_{abs} = \gamma T_{TES}$, to be around 0.40 pJ/K, which is quite close to the fitted C_{abs} , as shown in Fig. 5 a). The TES film heat capacity C_{TES} was also calculated with a correction¹³ to the BCS heat capacity jump for bilayer films, to get values around 0.08 pJ/K, which again agrees with our results. We see that the two model variants do not produce significant differences, and cannot be easily differentiated from each other. We do not want to draw conclusions from the bias dependence of the parameters yet, because we have evidence that the IH model is required even in devices without an absorber⁶.

In conclusion, good simultaneous fit to complex impedance and noise can only be achieved with a three-block model in these devices. The fitting parameter values are consistent with the heat capacities being the TES film, the absorber and a third

unknown heat capacity of the order of 0.1 pJ/K. No unexplained excess noise remains after the three-block fit.

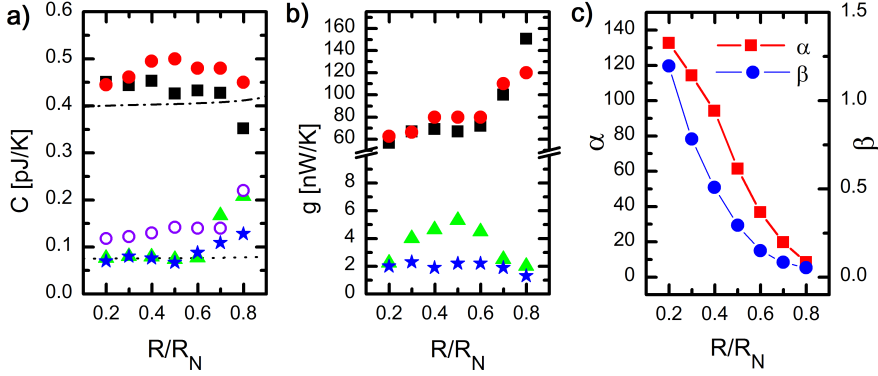


Fig. 5 (Color online) Some of the parameters from both IH and 2H models vs. bias point. a) C_{TES} (IH triangles, 2H stars), C_{abs} (IH squares, 2H circles) and C_{ex} (IH open circles) and the estimated theoretical values as dashed lines. b) g_{TES} (IH squares, 2H circles), g_0 (IH triangles) and g_{ex} (2H stars). c) α and β .

Acknowledgements This work was supported by ESA contract no AO/1-4005/01/NL/HB, the Finnish Funding Agency for Technology and Innovation TEKES and EU through the regional funds, and the Finnish Academy project no. 128532. M. P. would like to thank the National Graduate School in Materials Physics for funding.

References

1. K. Irwin and G. Hilton, in *Cryogenic Particle Detection* edited by. Ch. Enss, Springer, Berlin, 63 (2005).
2. J. N. Ullom, *et al.*, Appl. Phys. Lett. **84**, 4206 (2004).
3. K. M. Kinnunen, A. K. Nuottajärvi, J. Leppäniemi, and I. J. Maasilta, J. Low Temp. Phys. **151**, 119 (2008).
4. K. D. Irwin, Nucl. Instrum. Meth. A **559**, 718 (2006).
5. H. F. C. Hoevers, A. C. Bento, M. P. Bruijn, L. Gottardi, M. A. N. Korevaar, W. A. Mels, and P. A. J. de Korte, Appl. Phys. Lett. **77**, 4422 (2000).
6. K. M. Kinnunen, M. R. J. Palosaari, and I. J. Maasilta submitted for publication, arXiv:1111.4098v1.
7. M. Lindeman, *et al.*, Rev. Sci. Instrum. **75**, 1283 (2004).
8. I. J. Maasilta and K. M. Kinnunen, AIP Conf. Proc. **1185**, 38 (2009).
9. Y. Zhao, *et al.*, IEEE Trans. Appl. Supercond. **21**, 227 (2011).
10. I. J. Maasilta, to be published.
11. J. A. Chervenak, *et al.*, Appl. Phys. Lett. **74**, 4043 (1999).
12. Y. Takei, *et al.*, J. Low Temp. Phys. **151**, 161 (2008).
13. A. Kozorezov *et al.*, **1185**, 27 (2009).